

Stabilized Meshless Local Petrov-Galerkin (MLPG) Method for Incompressible Viscous Fluid Flows

M. Haji Mohammadi¹

Abstract: In this paper, the truly Meshless Local Petrov-Galerkin (MLPG) method is extended for computation of steady incompressible flows, governed by the Navier–Stokes equations (NSE), in vorticity-stream function formulation. The present method is a truly meshless method based on only a number of randomly located nodes. The formulation is based on two equations including stream function Poisson equation and vorticity advection-dispersion-reaction equation (ADRE). The meshless method is based on a local weighted residual method with the Heaviside step function and quartic spline as the test functions respectively over a local subdomain. Radial basis functions (RBF) interpolation is employed in shape function and its derivatives construction for evaluating the local weak form integrals. Due to satisfaction of Kronecker delta property in RBF interpolation, no special technique is employed to enforce the essential boundary conditions. In order to overcome instability and numerical errors (numerical dispersion) encountered in convection dominant flows, a new upwinding scheme is introduced and used to stabilize the convection operator in the streamline direction (as is done in SUPG). In this upwinding technique, instead of moving subdomains, the weight function is shifted in the direction of flow. Efficiency and accuracy of the new stabilization technique are investigated by a problem and compared with other stabilization techniques. In order to obtain the optimum parameters, Shape parameters of Multiquadric-RBF for both Poisson and convection-diffusion equations are tuned and studied. Effects of subdomain (integration domain) and support domain sizes are also studied. The efficiency, accuracy and robust-

ness of the modified MLPG are demonstrated by a well-known benchmark test problem including the standard lid driven cavity flow.

Keyword: Meshless local Petrov-Galerkin, Radial basis function, Multiquadrics, Upwind scheme, Vorticity-stream function

1 Introduction

The mostly used numerical methods consisting FEM, FDM, FVM and BEM have been utilized in two recent decades in computational mechanics. Among them, the finite element method (FEM) has been established as a very powerful numerical technique for the analysis of boundary value problems having arbitrary shapes. But it also has some drawbacks. It is an element-based method. In problems with need of remeshing, including time dependent problems, problems with moving boundaries and high gradients, it has been observed that mesh generation is a far more time-consuming and computationally expensive task than the assembly and solution of the system equations. Moreover, there are certain classes of problems, like problems with discontinuities and large deformations, for which FEM is difficult or even impossible to apply. These drawbacks made the researchers to introduce and develop a class of new methods, known as meshless methods. They may have different theory and background but they all have one property in common: They are node-based methods. This important feature is making these methods more popular. Domain and its boundaries are represented by some randomly scattered nodes (or particles). Unlike FEM, no connectivity among nodes is required which leads to flexibility in removing or adding nodes. Meshless

¹ Sharif University of Technology, Tehran, IRAN

methods are usually categorized in two groups: strong form based and weak form based methods. In the strong form methods the equilibrium equations are satisfied on each node (or particle) like smooth particle hydrodynamics (SPH), which were first applied for astrophysics problems by Gingold and Monaghan (1977), and finite point method (FPM), applied for fluid flow by Onate, Idelsohn, Zienkiewicz and Taylor (1996). In the weak form methods the equations are satisfied on the global domain in an integral sense. Various meshless methods belonging to this family are diffuse element method (DEM), first introduced by Nayroles, Touzot, and Villon (1992), reproducing kernel particle method [see Liu, Jun and Zhang (1995)], element-free Galerkin (EFG) method by Belytschko, Lu and Gu (1994) which is considered as extension of DEM method, the partition of unity method (POU) by Babuska and Melenk (1997), extended finite element method (XFEM) by Daux, Mose, Dolbow, Sukumar and Belytschko (2000), and natural element method and so on. Global weak form (GWF) methods are not "truly meshless" methods as long as they require a virtual mesh called background cell for computation of integrals over the global domain in the system stiffness matrix. Recently a group of meshless methods based on local weak form (LWF) of equations are introduced and developed. These methods include meshless local Petrov-Galerkin (MLPG), which were first introduced and utilized by Atluri and his colleagues [see Atluri and Zhu (1998), Atluri and Zhu (2000) and Atluri and Shen (2002)], local boundary integral equation (LBIE) by Zhu, Zhang and Atluri (1998) [also see Vavourakis, Sellountos and Polyzos (2006)] and method of finite spheres by De and Bathe (2000).

These methods are "truly meshless" because they don't need any "element" or "mesh" for either field interpolation or background integration. Equilibrium in these methods is satisfied in a local sense on subdomains or integration domains. These local domains can be as simple as circles or rectangles in two-dimension and ellipsoid or sphere in 3-D domains and can also have different sizes which lead to flexibility in dealing with

non-linear problems.

In the MLPG method some form of Petrov-Galerkin formulation of equations is utilized which means that functions from different spaces for trial and test function are deliberately adopted. Trial function approximation is usually performed by moving least squares (MLS), partition of unity and radial basis functions (RBF). Unlike MLS, employing RBF needs no special effort to enforce essential boundary conditions. The test functions are employed in a manner to most simplify the stiffness matrix components.

Remarkable success in MLPG method and its application in computational mechanics have been reported. Considerable efforts have been made to use the MLPG method to solve problems in the solid mechanics field [see Long and Atluri (2002), Xiao (2004), Atluri, Liu and Han (2006) and Jarak, Sori'c and Hoster (2007)] while few articles are involved in computational fluid dynamics (CFD). The first paper on MLPG in CFD was written by Lin and Atluri (2001) in which stokes flow and cavity problem were studied by MLPG with moving least squares approximation. In their work, two upwinding schemes (USI, USII) were introduced and applied into the MLPG method. The governing equations were based on the primitive variables formulation and to satisfy the Babuska-Brezzi conditions, they added a perturbation term to continuity equation and found that determining stability parameter β is difficult. They considered the problem to $Re=400$. In addition, their computations validated the MLPG method only with uniformly distributed nodes. Due to dissatisfaction of kronecker property in MLS, the boundary conditions of Dirichlet type were imposed by transformation method. The other work was done by Wu, Liu and Gu (2005). They employed MLPG method with MLS approximation to solve flow in concentric annulus but no stabilization technique was used. Arefmanesh, Najafi and Abdi (2008) solved the N-S equations with energy equation for non-isothermal fluid flow. They considered the lid driven cavity flow and flow over an obstacle as their problem with standard upwinding technique. Sladek, J.; Sladek, V. and Atluri (2004)

applied MLPG method to solve the heat conduction problem in an anisotropic medium. In their work, Heaviside step function together with moving least squares (MLS) method has been employed to obtain the discretized form of equations.

In a recent work by Wu, Shen and Tao (2007), MLPG was applied to two dimensional heat conduction problems. They utilized the Dirac's Delta function as the test function in their formulation and compare their results with that of a commercial CFD package.

Ma (2005a) extended the MLPG method to simulating nonlinear water waves and produced some encouraging results. In that paper, the simple Heaviside step function was adopted as the test function to formulate the weak form over local sub-domains, resulting in equations in terms of pressure gradient. The formulation is based on general fluid governing equations and a time marching procedure. At each time step, the boundary value problem for the pressure is solved using the MLPG method and the velocity and position of nodes are updated by numerical integration.

Ma (2005b) employed the MLPG method based on Rankine source solution for simulating transient nonlinear water waves generated by wave makers. In that paper, the solution for Rankine sources rather than the Heaviside step function was adopted as the test function to formulate the weak form over local subdomains, resulting in a weak form of governing equations which did not contain the gradients of unknown functions. In another work by Ma (2008), the so called simplified finite difference interpolation (SFDI) was devised and successfully applied to MLPG based on Rankine source solution (MLPG-R).

In this paper some modifications into the MLPG method is introduced, involving a new stabilization technique in convection dominated flows, and applied it to fluid flow problems to verify the new upwinding scheme. Radial basis function of multiquadric type is adopted as meshless interpolation method. Then modified MLPG formulation is applied to simulation of flow in cavity with Reynolds number of as high as $Re=10000$ and compared with certified data of U. Ghia, K.N.

Ghia and Shin (1982). The results demonstrate very clearly that the RBF-MLPG method with the new stabilization technique, as a mesh-free method, can treat problems with high accuracy and without any difficulty.

2 Radial basis function (RBF) interpolation

Like other meshless methods, the MLPG method requires a local node-based interpolation or approximation to represent the trial function. The local approximation schemes like MLS, PUM, and RKPM use fictitious values at scattered nodes, and the local interpolation schemes like PIM and RBFs enable trial functions that pass through the actual values of the unknown variables at scattered nodes, i.e. shape functions constructed satisfy kronecker delta property. A major drawback of PIM method is the possibility of moment matrix to be singular or ill-conditioned. It has been proved that RBFs do not face the mentioned problem as long as specific values of shape parameters are not applied. Also use of RBFs leads to symmetric moment matrix, convergent and more stable interpolation. Radial basis functions were introduced by Hardy in 1971 for the first time and employed to solution of PDE in strong form. Then it was developed for meshless methods [see Sarler (2005), Zhang, Song, Lu, and Liu (2000) and Chantasiriwan (2006)]. A comprehensive study of RBFs is accomplished by Hoo (2004). In his report, he performed studies on the various RBFs to find out their properties and the best shape parameters through the surface fitting and solution of a 2-D Solid Mechanics problem.

A continuous function $u(x)$ defined in a domain Ω discretized by a set of nodes can be interpolated from the neighboring nodes of a point \mathbf{x}_Q using radial basis functions as

$$u^h(\mathbf{x}, \mathbf{x}_Q) = \sum_{i=1}^n g_i(\mathbf{x}) \bar{a}_i(\mathbf{x}_Q) = \mathbf{G}^T(\mathbf{x}) \mathbf{a}(\mathbf{x}_Q) \quad (1)$$

where $g_i(\mathbf{x})$ is the radial basis function in the space coordinates $\mathbf{x}^T = [x, y]$, n is the number of nodes in the neighborhood (refers to support domain) of \mathbf{x}_Q , and $\bar{a}_i(\mathbf{x}_Q)$ are the coefficients for $g_i(\mathbf{x})$, respectively, corresponding to the given point \mathbf{x}_Q . It should be noted that the number (n) of

the neighboring nodes of \mathbf{x}_Q is less than or equal to the total number of nodes in the global problem domain (n_t) depending on the size of support domain specified. The vectors are defined as:

$$\bar{\mathbf{a}} = [\bar{a}_1, \bar{a}_2, \bar{a}_3, \dots, \bar{a}_n]^T \quad (2)$$

$$\mathbf{G}^T = [g_1(\mathbf{x}), g_2(\mathbf{x}), g_3(\mathbf{x}), \dots, g_n(\mathbf{x})]^T \quad (3)$$

The radial distance function in a two dimensional domain is a function of Euclidean distance r defined as:

$$r_i = [(x - x_i)^2 + (y - y_i)^2]^{\frac{1}{2}} \quad (4)$$

Here another important advantage of RBFs emerges: the radial distance function transforms a multiple dimensional problem into one dimension. Enforcing the interpolation to pass through all n scattered nodes within the point \mathbf{x}_Q support domain leads to the following set of equations for the coefficients $\bar{a}_i(\mathbf{x}_Q)$:

$$u_k = u(y_k, z_k) = \sum_{i=1}^n \bar{a}_i(\mathbf{x}_Q) g_i(y_k, z_k), \quad k = 1, 2, 3, \dots, n \quad (5)$$

This can be expressed in matrix form as follows

$$\mathbf{A} \mathbf{a} = \mathbf{U}_s \quad (6)$$

where $\mathbf{U}_s = [u_1, u_2, u_3, \dots, u_n]$ and \mathbf{A} is the symmetric interpolation matrix of rank $(n \times n)$ as follows

$$\mathbf{A} = \mathbf{A}^T = \begin{bmatrix} g_1(r_1) & g_2(r_1) & \dots & g_n(r_1) \\ g_2(r_2) & g_2(r_2) & \dots & g_n(r_2) \\ \vdots & \vdots & \ddots & \vdots \\ g_1(r_n) & g_2(r_n) & \dots & g_n(r_n) \end{bmatrix} \quad (7)$$

The coefficients can be obtained as

$$\mathbf{a} = \mathbf{A}^{-1} \mathbf{U}_s \quad (8)$$

where \mathbf{A}^{-1} is the inverse matrix of \mathbf{A} .

Finally, the interpolation can be expressed as

$$u^h(\mathbf{x}) = \mathbf{G}^T(\mathbf{x}) \mathbf{A}^{-1} \mathbf{U}_s = \Phi(\mathbf{x}) \mathbf{U}_s \quad (9)$$

$\Phi(\mathbf{x})$ is the vector of shape functions defined as

$$\Phi(\mathbf{x}) = [\phi_1(\mathbf{x}), \phi_2(\mathbf{x}), \phi_3(\mathbf{x}), \dots, \phi_k(\mathbf{x}), \dots, \phi_n(\mathbf{x})] \quad (10)$$

in which

$$\phi_k(\mathbf{x}) = \sum_{i=1}^n g_i(\mathbf{x}) \bar{A}_{i,k} \quad (11)$$

and $\bar{A}_{i,k}$ is the (i, k) component of the matrix \mathbf{A}^{-1} . The derivatives of $\phi_k(\mathbf{x})$ can be obtained as follows:

$$\frac{\partial \phi_k}{\partial x} = \sum_{i=1}^n \frac{\partial g_i}{\partial x} \bar{A}_{i,k} \quad (12a)$$

$$\frac{\partial \phi_k}{\partial y} = \sum_{i=1}^n \frac{\partial g_i}{\partial y} \bar{A}_{i,k} \quad (12b)$$

RBFs are classified into two categories: classic RBFs (globally supported RBFs) and compactly supported RBFs (CSRBF). For through investigation on CSRBF, the reader may refer to Wu (1995), Wendland (1995) and Hoo (2004). The most important three classical RBFs are consisted of Multiquadrics (MQ), Gaussian (EXP) and thin plate splines (TPS) as follows:

$$\begin{aligned} g_i(y, z) &= (r_i^2 + C^2)^\beta & (\mathbf{MQ}) \\ g_i(y, z) &= (r_i)^\eta \log r_i & (\mathbf{TPS}) \\ g_i(y, z) &= e^{-c^2 r_i^2} & (\mathbf{EXP}) \end{aligned} \quad (13)$$

where β , C and η are shape parameters that are used for fine tuning. Among them, MQ is utilized more frequently and proved to have exponential convergence. The partial derivatives of MQ-RBF are as follows:

$$\begin{aligned} \frac{\partial g_i}{\partial x} &= 2\beta (r_i^2 + C^2)^{\beta-1} (x - x_i) \\ \frac{\partial g_i}{\partial y} &= 2\beta (r_i^2 + C^2)^{\beta-1} (y - y_i) \end{aligned} \quad (14)$$

Fig. 1 shows typical shape functions for two-dimensional problem using MQ basis within a domain containing 7×7 nodes only in a $[-1, 1] \times [-1, 1]$ $x - y$ space. According to G.R. Liu's recommend, the shape parameters are chosen $\alpha_c = 1.42$

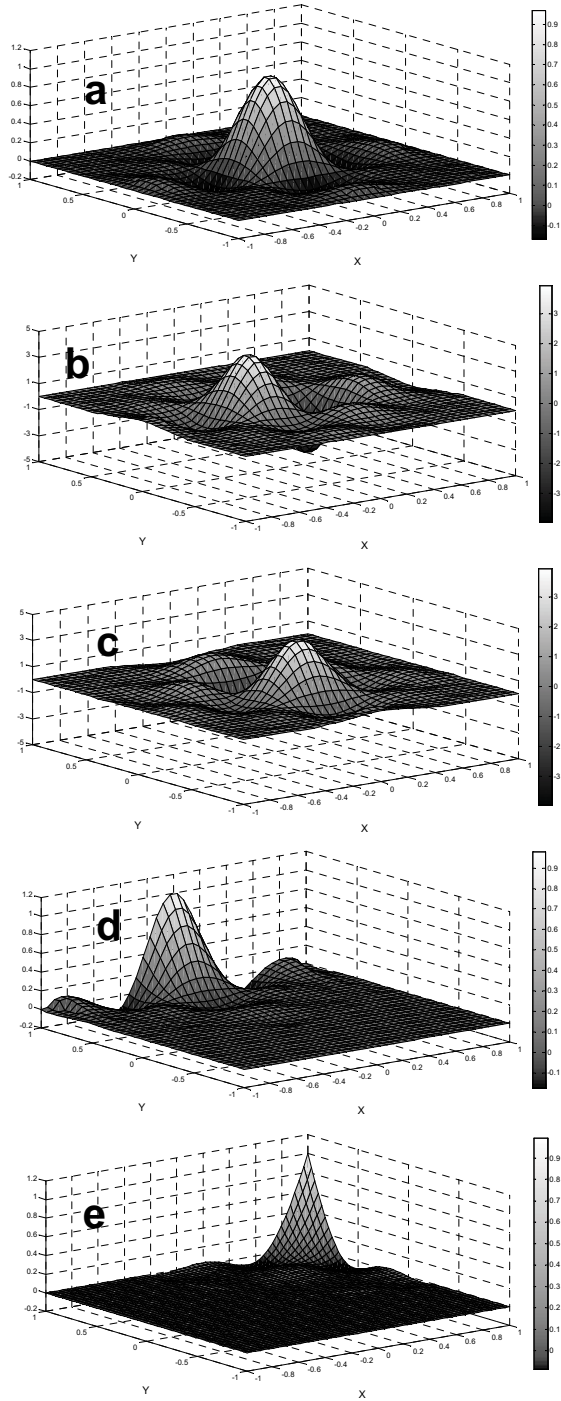


Figure 1: MQ-RBF shape functions for two-dimensional domain (49 nodes). **a)** Shape function of central node; **b), c)** shape function x , y -derivative of central node; **d), e)** Shape function for an edge and corner node

and $\beta = 1.03$. For better compatibility, the dimensionless size of support domain is $\alpha_s = 3.7$.

All the shape functions satisfy the kronecker delta function property which makes imposition of essential boundary conditions as easy as FEM. As is obvious, both shape function and the derivatives are smooth functions and unlike FEM need not any smoothing technique. Due to a local interpolation, the shape functions have zero value immediately outside the local support domain.

3 Governing equations

The dimensionless non conservative two-dimensional Navier–Stokes equations in form of the vorticity–stream function formulation within closed domains in Cartesian coordinate system are as follows:

$$\frac{\partial^2 \psi}{\partial x^2} + \frac{\partial^2 \psi}{\partial y^2} = -\omega \quad (15)$$

$$\frac{\partial \omega}{\partial t} + u \frac{\partial \omega}{\partial x} + v \frac{\partial \omega}{\partial y} = \frac{1}{Re} \left[\frac{\partial^2 \omega}{\partial x^2} + \frac{\partial^2 \omega}{\partial y^2} \right] \quad (16)$$

where ω , ψ and Re are the vorticity, stream function and Reynolds number. u , v are the components of velocity in the x and y directions, which can be calculated using

$$u = \frac{\partial \psi}{\partial y}; \quad v = -\frac{\partial \psi}{\partial x} \quad (17)$$

One of the advantages of using Vorticity–Stream function formulation lies in removing pressure gradient terms from the solution process, resulting in a higher numerical stability of the computational scheme. The pressure does not appear in the solution procedure and has no influence on the velocity field, a fact that is of course valid only for incompressible fluid approximation. The pressure can be computed, after obtaining velocity field, by the Poisson pressure equation:

$$\frac{\partial^2 p}{\partial x^2} + \frac{\partial^2 p}{\partial y^2} = 2 \left[\left(\frac{\partial^2 \psi}{\partial x^2} \right) \left(\frac{\partial^2 \psi}{\partial y^2} \right) - \left(\frac{\partial^2 \psi}{\partial x \partial y} \right)^2 \right] \quad (18)$$

In MLPG, the error of dissatisfaction of equations on subdomains are made zero. This is the

most distinctive feature of the MLPG. Also, it will lead to a natural way to construct the global stiffness matrix. This is because of satisfaction of equations only over subdomains, not on whole domain. Consequently the assembly process is much less costly than other GWF methods like FEM or EFG whereas the assembly process is analogous to FDM.

In the following sections the formulation of Eqs. 15 and 16 are presented separately.

3.1 Poisson equation

The 2-D Poisson equation of streamline is considered where ω is treated as a given source term. The domain Ω is enclosed by $\Gamma = \Gamma_u \cup \Gamma_q$, with boundary conditions

$$\psi_i = \bar{\psi}_i \quad \text{on } \Gamma_u \quad (19a)$$

$$\left. \frac{\partial \psi}{\partial n} \right|_i = \bar{q}_i \quad \text{on } \Gamma_q \quad (19b)$$

where Γ_u is the essential boundary and Γ_q is the boundary with predefined flux.

A general weak form of Eq. 15 by applying the weighted residual method locally over the quadrature domain and employing divergence theorem leads to

$$-\int_{\Omega_Q} (W_{,x} \psi_{,x} + W_{,y} \psi_{,y}) d\Omega + \int_{\Gamma_Q} W \frac{\partial \psi}{\partial n} d\Gamma = -\int_{\Omega_Q} W \omega d\Omega \quad (20)$$

where ψ is the trial function, Γ_Q is the boundary of the quadrature domain Ω_Q , n is the outward unit normal to the boundary Γ_Q and W is the test function.

Imposing the natural boundary condition, Eq. 19b, one obtains

$$-\int_{\Omega_Q} (W_{,x} \psi_{,x} + W_{,y} \psi_{,y}) d\Omega + \int_{\Gamma_{Qu}} W \frac{\partial \psi}{\partial n} d\Gamma + \int_{\Gamma_{Qi}} W \frac{\partial \psi}{\partial n} d\Gamma = -\int_{\Omega_Q} W \bar{q} d\Gamma - \int_{\Omega_Q} W \omega d\Omega \quad (21)$$

in which Γ_{Qi} is a part of Γ_Q , over which the natural boundary condition is specified; Γ_{Qu} is the

intersection of Γ_Q and the essential boundary Γ_u ; Γ_{Qi} is the internal part of Γ_Q on which no boundary condition is specified, as shown in Fig. 2. For a quadrature domain located entirely within the global domain, there is no intersection between Γ_Q and Γ , and the integrals over Γ_{Qu} and Γ_{Qi} vanish.

Different test function W with the constraint to be at least C^1 can be chosen. Atluri and Shen (2002) tested different test functions and showed that Heaviside step function is the best for potential problems which leads to symmetric stiffness matrix. Using this weight function, Eq. 21 is rewritten as

$$\int_{\Gamma_{Qu}} \frac{\partial \psi}{\partial n} d\Gamma + \int_{\Gamma_{Qi}} \frac{\partial \psi}{\partial n} d\Gamma = -\int_{\Gamma_{Qq}} \bar{q} d\Gamma - \int_{\Omega_Q} \omega d\Omega \quad (22)$$

It can be seen that the domain integral is avoided and only the regular boundary integral along the boundaries of subdomains is involved.

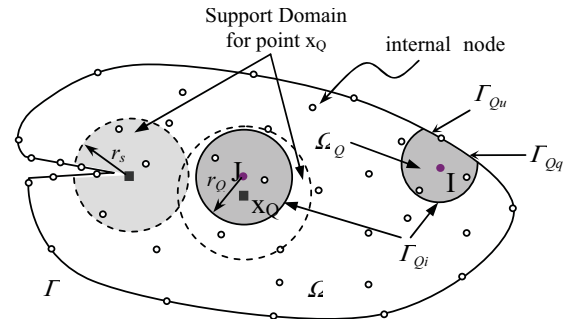


Figure 2: The support domain and quadrature domain in constructing the discretized equation for node I

The LSWF, Eq. 22, gives one algebraic equation relating all ψ_i . Thus, one should obtain as many equations as the number of nodes. Therefore, we need as many local domains Ω_Q as the number of nodes in the global domain.

To obtain the discrete equations from the LSWF (22), the radial basis function interpolation is adopted to approximate the trial function ψ . Substitution of Eq. 9 into Eq. 22 for all nodes leads

to the following discretized system of linear equations:

$$[\mathbf{K}] \{\bar{\boldsymbol{\psi}}\} = \{\mathbf{f}\} \quad (23)$$

where $[\mathbf{K}]$ and $\{\mathbf{f}\}$ are "stiffness" matrix and the "load" vector, respectively, defined as

$$K_{IJ} = \int_{\Gamma_{Q_i}} (\phi_{J,x} n_x + \phi_{J,y} n_y) d\Omega + \int_{\Gamma_{Q_u}} (\phi_{J,x} n_x + \phi_{J,y} n_y) d\Omega \quad (24a)$$

$$f_I = - \int_{\Omega_Q} \omega(x,y) d\Omega - \int_{\Gamma_{Q_q}} \bar{q} d\Omega \quad (24b)$$

Gauss quadrature is employed in each local sub-domain centered at node \mathbf{x}_i . For each Gauss quadrature point \mathbf{x}_Q , RBF is performed to obtain the integrand. Therefore, for a node \mathbf{x}_i , there are two local domains: the test function domain Ω_{te} (same as the local sub-domain Ω_Q) for $\mathbf{W}_i \neq 0$ (size \mathbf{r}_Q), and the interpolation domain Ω_s for \mathbf{x}_Q (size \mathbf{r}_s).

Fig. 2 shows the quadrature domain Ω_Q of a node \mathbf{x}_i and the support domain Ω_s for a gauss point \mathbf{x}_Q . These two domains are independent and defined as $\mathbf{r}_s = \alpha_s dc$ and $\mathbf{r}_Q = \alpha_Q dc$, respectively, where α_s and α_Q are dimensionless coefficients and dc known as characteristic length is the shortest spacing between node i and its neighbor nodes or the global boundary whichever is smaller. Parameters including shape parameters of RBFs and parameters related to MLPG (support and sub-domain size) should be tuned. In a paper by Haji Mohammadi and Shamsai (2006) these optimum values were obtained for the poisson equation which were defined as follows

MQ-RBF: $\alpha_c=5.54$, $\beta=1.03$, 0.98 ; MLPG: $\alpha_Q=0.82$, $\alpha_s=3.5$

3.2 Vorticity transport equation

The convection operator in Eq. 16 makes the equation non self adjoint i.e. the weak form can not be written symmetrically with respect to test and trial functions. Due to existence of this term, in all numerical methods, one encounters a numerical error nominated as numerical dispersion

which leads to oscillatory solutions for vorticity. Therefore some techniques were introduced in literature for FEM like FIC (finite increment calculus) and SUPG (streamline upwind Petrov-Galerkin). The last one is the mostly used technique rather than others. In this section the formulation of Eq. 16 is presented and a novel up-winding technique is introduced in advance.

The boundary conditions are assumed to be:

$$\omega_i = \bar{\omega}_i \text{ on } \Gamma_\omega \text{ (Dirichlet B.C.)} \quad (25a)$$

$$\frac{1}{Re} \frac{\partial \omega}{\partial \mathbf{n}} \Big|_i = \bar{t}_i \text{ on } \Gamma_t \text{ (Neumann B.C.)} \quad (25b)$$

where, $\bar{\omega}$ and \bar{t} are given, \mathbf{n} is the outward unit normal vector to Γ , Γ_ω and Γ_t are part of boundary Γ satisfying $\Gamma_\omega \cap \Gamma_t = 0$ and $\Gamma_\omega \cup \Gamma_t = \Gamma$.

A general local weak form of Eq. 16, by applying the weighted residual method over the quadrature domain, can be written as

$$\int_{\Omega_Q} W \left(\frac{\partial \omega}{\partial t} + u \frac{\partial \omega}{\partial x} + v \frac{\partial \omega}{\partial y} - \frac{1}{Re} \nabla^2 \omega \right) d\Omega = 0 \quad (26)$$

By using the divergence theorem and directly imposing the Neumann boundary condition, the following local symmetric weak form is obtained

$$\begin{aligned} & \int_{\Omega_Q} W \left(u \frac{\partial \omega}{\partial x} + v \frac{\partial \omega}{\partial y} \right) d\Omega \\ & + \frac{1}{Re} \int_{\Omega_Q} \left(\frac{\partial W}{\partial x} \frac{\partial \omega}{\partial x} + \frac{\partial W}{\partial y} \frac{\partial \omega}{\partial y} \right) d\Omega \\ & - \frac{1}{Re} \int_{\Gamma_{Q_i}} W \bar{t} d\Gamma - \frac{1}{Re} \int_{\Gamma_{Q_i}} W \frac{\partial \omega}{\partial \mathbf{n}} d\Gamma \\ & - \frac{1}{Re} \int_{\Gamma_{Q_\omega}} W \frac{\partial \omega}{\partial \mathbf{n}} d\Gamma + \int_{\Omega_Q} W \dot{\omega} d\Omega = 0 \quad (27) \end{aligned}$$

temporal discretization is implemented by the Euler scheme

$$\dot{\omega} = \frac{\partial \omega}{\partial t} = \frac{\omega^n - \omega^{n-1}}{\Delta t} \quad (28)$$

Consequently, the system stiffness matrix and

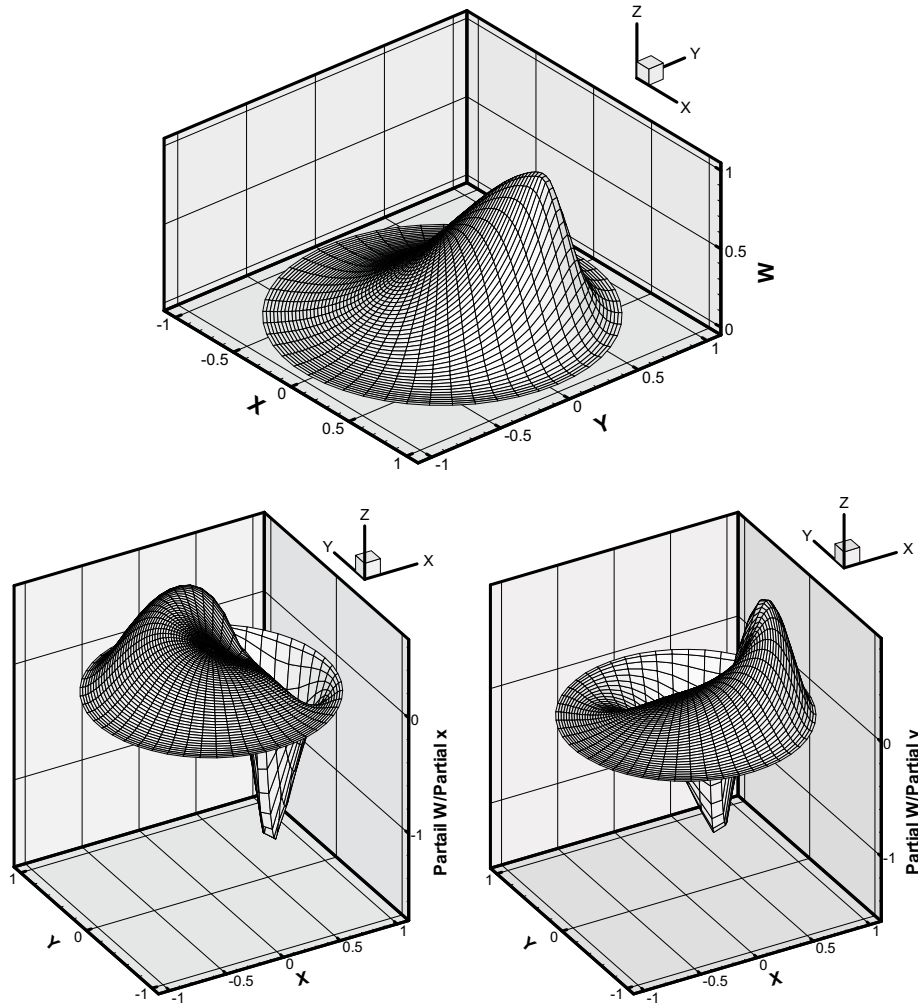


Figure 3: Test function and its derivatives in USI

load vector are obtained as below

$$\begin{aligned}
 [\mathbf{K}]_{ij} &= Re \int_{\Omega_Q} [u\phi_{j,x} + v\phi_{j,y}] W d\Omega \\
 &+ \int_{\Omega_Q} (W_{,x}\phi_{,x} + W_{,y}\phi_{,y}) d\Omega \\
 &- \int_{\Gamma_{Q_u}} W \frac{\partial \phi_j}{\partial \mathbf{n}} d\Gamma - \int_{\Gamma_{Q_v}} W \frac{\partial \phi_j}{\partial \mathbf{n}} d\Gamma \\
 &\quad + \frac{Re}{\Delta t} \int_{\Omega_Q} \phi_j W d\Omega \quad (29a)
 \end{aligned}$$

$$\{\mathbf{f}\}_i = \int_{\Gamma_{Q_i}} W \bar{\tau} d\Gamma + \frac{Re}{\Delta t} \int_{\Omega_Q} W \omega^{n-1} d\Omega \quad (29b)$$

In order to simplify the above equation, we deliberately select a test function \mathbf{W} such that it vanishes over Γ_{Q_i} . This can be easily accomplished

by using the quartic spline as the weight function

$$\hat{W}(\mathbf{x}_Q - \mathbf{x}_i) = \begin{cases} 1 - 6\bar{d}^2 + 8\bar{d}^3 - 3\bar{d}^4 & 0 \leq \bar{d} \leq 1 \\ 0 & \bar{d} \geq 1 \end{cases} \quad (30)$$

4 Upwinding technique

In convection dominated flows, the presence of the convection term causes serious numerical difficulties, appearing in the form of oscillatory solutions. Several attempts have been made to remove or at least alleviate this problem. The solutions proposed were based on upwinding concepts. Upwind effect was needed only in the direction of flow that led to SU (streamline up-

wind) scheme. For consistency purposes, upwind weighting of all terms in the equation was needed, i.e., some kind of Petrov-Galerkin method is needed. Therefore another version of stabilization scheme called Streamline Upwind Petrov-Galerkin method (SUPG) was introduced which consistently utilized an additional stability term in the upwind direction. This method has better stability and accuracy properties than the standard Galerkin formulation for convection-dominated flows.

For meshless methods, the same kind of consideration should be taken to deal with convection-dominated flows. As mentioned by Atluri, the very general nature of truly meshless methods, such as the MLPG method, makes it easier to introduce the upwind concept more clearly and effectively.

The pioneering work on upwinding in MLPG belongs to work of Lin and Atluri (2000). They suggested two techniques of which the second one (USII) gained better results. In the following their method is described and the new modified technique is also introduced.

In USI, test function and quadrature domain spaces do not change but the test function is skewed opposite to the streamline direction. The process is shown in Fig. 3.

In the method suggested by Lin and Atluri as USII, shown in Fig. 4, the upwinding was applied to subdomains where

$$\gamma = \coth(Pe/2) - 2/Pe \quad (31)$$

$$Pe = 2 \left\| \vec{V} \right\| r(Re) \quad (32)$$

The technique is somewhat not suitable for MLPG because for nodes near the boundary the upwinded subdomains may intersect with the global boundary. Furthermore it is not fully consistent with MLPG programming.

In our proposed scheme, it is suggested that instead of moving the subdomains, the weight function is shifted which is easier to implement in MLPG. The new scheme is named as upwinding scheme III (USIII). Fig. 5 illustrates this process

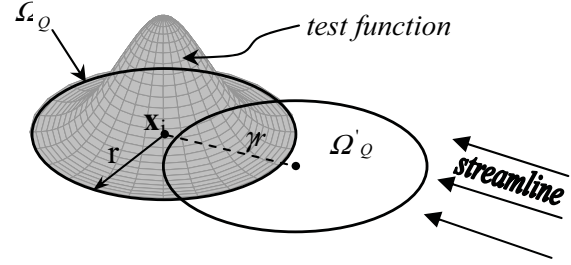


Figure 4: MLPG upwind (USII) suggested by Lin & Atluri

in which

$$\gamma = (1/2) \coth(Pe/2) - 1/Pe \quad (33)$$

In MLPG, the equations are satisfied locally node by node on the quadrature domains. Therefore in the new technique parts of weight functions that are out of the quadrature domain are not considered in the computation which leads to a more efficient method.

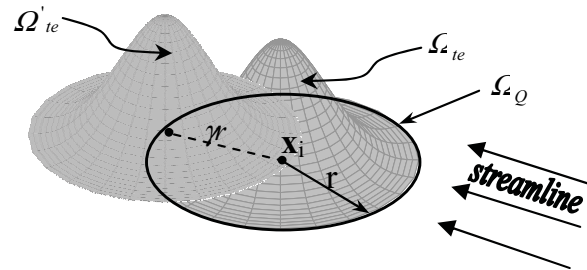


Figure 5: The new proposed MLPG upwinding (USIII)

5 Numerical examples

MLPG method with radial basis functions has some parameters. These parameters should be tuned and their behaviors to be studied. Therefore a problem with body term

$$f(x, y) = u \exp(x) + 3vy^2 - K (\exp(x) + 6y), \quad 0 \leq x, y \leq 2$$

is considered. Circular quadrature and support domains are utilized. Domain, subdomains and the nodes distribution are illustrated in Fig. 6.

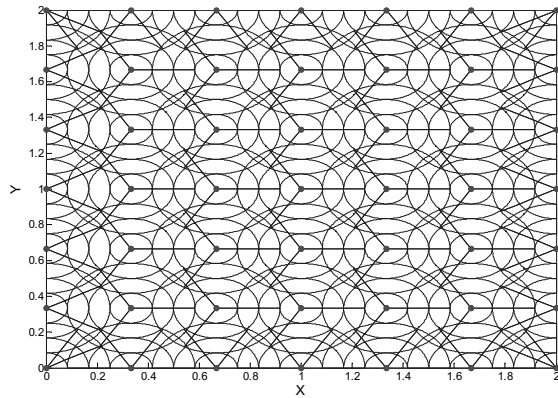


Figure 6: Domain and nodes distribution

In order to study multiquadric shape parameters we limit the parameter β to $[-0.5, 5]$ and α_c to $[0.3, 6]$. Variation of L_2 error norm versus β is demonstrated in Fig. 7.

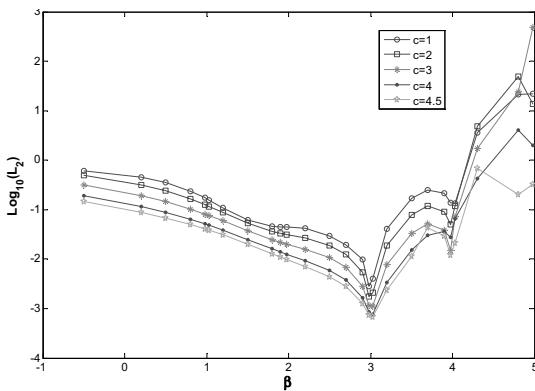


Figure 7: Effect of shape parameter β on $\|L_2\|$

According to the figure, $\beta = 2.98, 3.03$ are optimum values for convection-diffusion equation. It is worth noting that β can't be an integer otherwise moment matrix will be singular. Effect of α_c parameter versus L_2 norm is demonstrated in Fig. 8.

As shown, up to $\alpha_c = 5.2$, the accuracy increases continuously as α_c increases and above that accuracy decreases for two values of $\beta = 2.98, 3.03$.

To study the effect of quadrature domain size, we limit its non dimensional size to be larger than zero and less than one. Limiting the size less than unity makes the subdomains not to intersect with

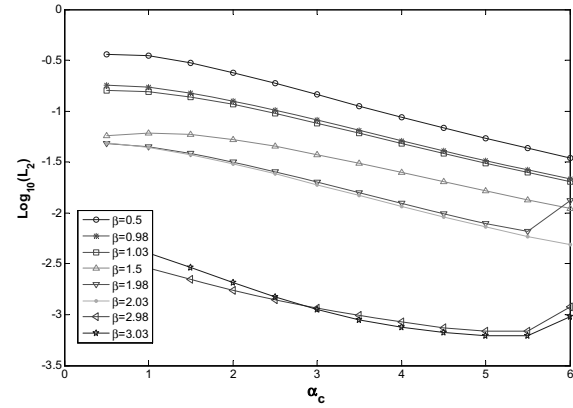


Figure 8: Effect of shape parameter α_c on $\|L_2\|$

global boundary and hence the integrals (29) are computed more easily for internal nodes. Quadrature domains with different sizes are examined and the L_2 errors are plotted in Fig. 9.

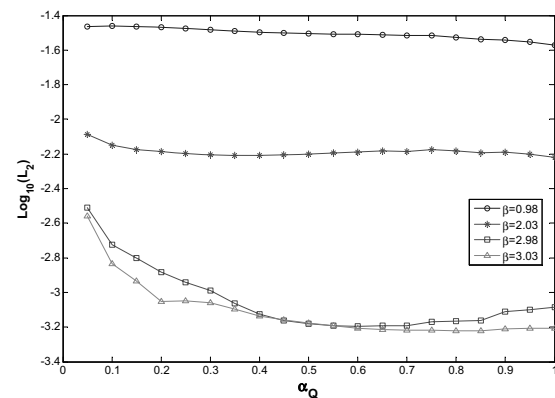


Figure 9: Effect of quadrature domain size α_Q on $\|L_2\|$

It can be seen that stable results are obtained when α_Q varies from 0.35 to 0.85. However best accuracy and stability was gained by $\alpha_Q = 0.75$.

The size of support domain α_s is an important parameter in all meshless methods because it relates to both accuracy and efficiency. A too large support domain leads to inefficient computations while too small one results in inaccurate and erroneous solutions. The L_2 norms for $\alpha_s = 1.5-7$ are obtained and plotted in Fig. 10.

For small values of α_s there is not enough nodes to perform interpolation. Upto a certain magni-

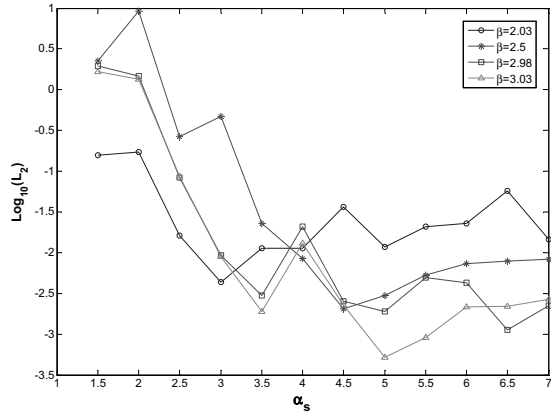


Figure 10: Variation of $\|L_2\|$ with support domain size α_s

tude of α_s , the results improve as α_s increases. Enlarging more does not necessarily improve the solution but makes the bandwidth of moment matrix larger. According to the above figure, α_s in the range [5, 5.5] is considered optimum.

In order to view and compare different upwinding schemes, a problem in a unit square, which were considered by Lin and Atluri (2000), is solved by MLPG-RBF with different schemes. The parameters are utilized as below

$$\alpha_s = 5.3; \quad \alpha_Q = 0.75; \quad \alpha_c = 5.15;$$

$$\beta = 3.03; \quad nc_\theta = nc_r = 4$$

Body force term is considered zero and velocity components are assumed to be $u = \cos(\pi/4)$; $v = \sin(\pi/4)$. Domain and its corresponding boundary conditions are depicted in Fig. 11, where ϕ is the field variable.

This problem was considered for different values of Peclet number. The field variable contours for $Pe = 1, 100, 10^6$ are presented in Figs. 12, 13 and 14, respectively.

As shown, for low Peclet numbers, all techniques and Galerkin finite element method yield good solutions. Numerical errors emerge as Peclet number increases. It can be seen that for high Peclet numbers, MLPG with radial basis functions are superior to FEM and MLPG with moving least squares [see Lin and Atluri (2000)]. Also, among three stabilization techniques, obviously USIII re-

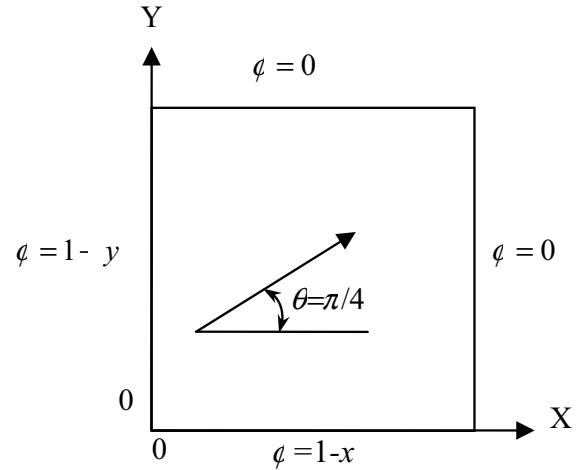


Figure 11: Domain and its boundary conditions

sults in more accurate and less oscillatory solutions.

6 Test problem

Fluid flow in a square cavity is one of the most difficult benchmark problems in flows of incompressible fluids, which is currently used for testing different numerical schemes for solution of Navier–Stokes equations. Numerous studies have been accomplished for the so called lid driven cavity problem. A comprehensive survey and literature review can be found in Erturk, Corke and Gokcol (2005).

7 Boundary conditions

The type and imposition of boundary conditions method is similar to the work done by Wu, Liu and Gu (2005). The procedure is described below. Suppose w is a node on boundary where the vorticity is to be determined as boundary condition. i is the nearest internal node to w in the direction of $-\mathbf{n}_w$ where \mathbf{n}_w is the unit normal vector to boundary at w . Distance of w and i is considered as l . According to Eq. 15, it is observed that obtaining boundary condition of vorticity is equal to 2^{nd} order derivatives approximation of stream function on the boundary (node w). As long as the walls are vertical, one can write

$$\Omega = -(\partial^2 \psi / \partial \mathbf{n}^2)_w \quad (34)$$

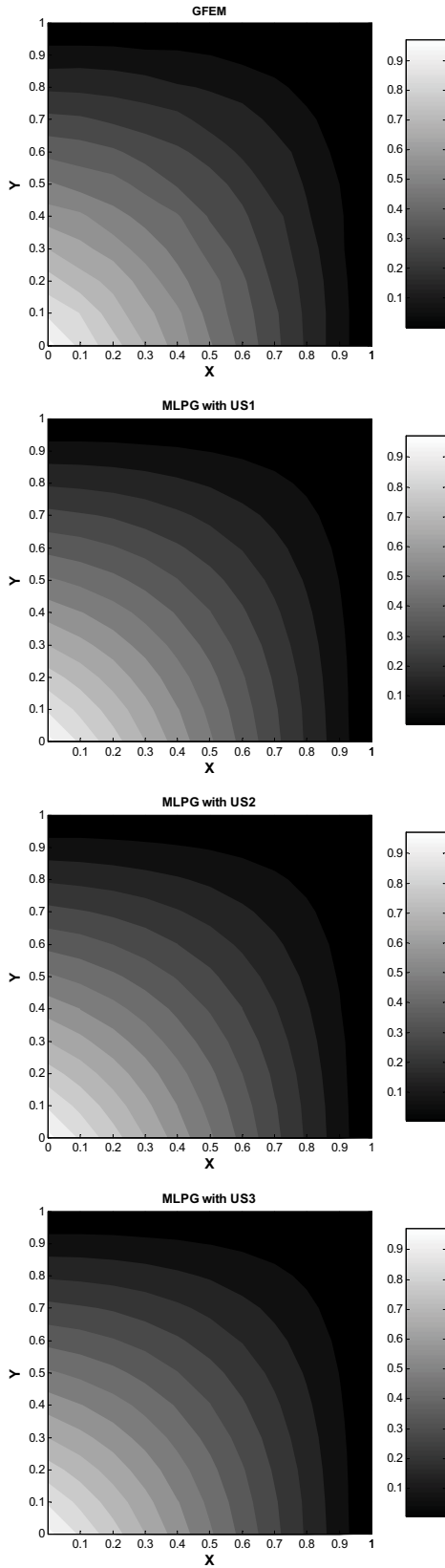


Figure 12: Field variable contours for $Pe = 1$

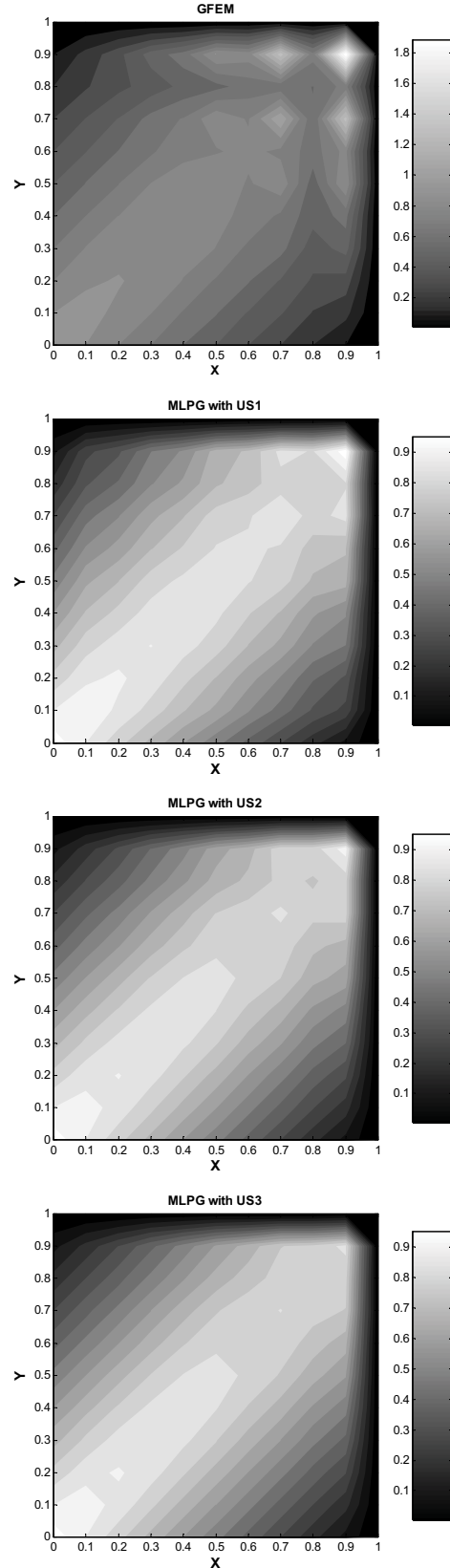


Figure 13: Field variable contours for $Pe = 100$

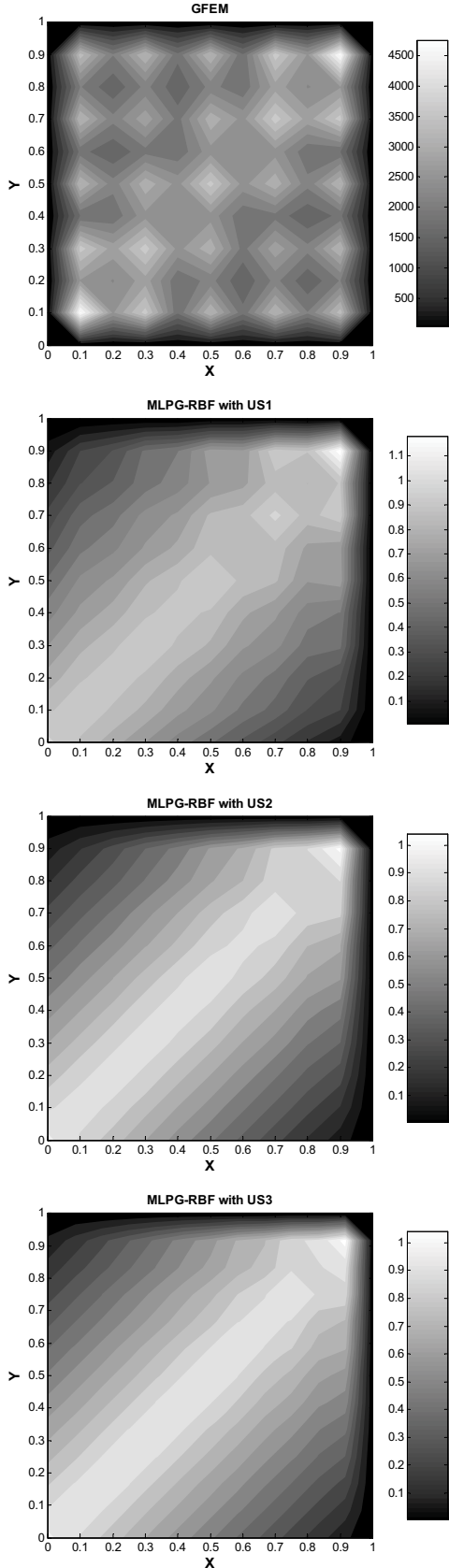
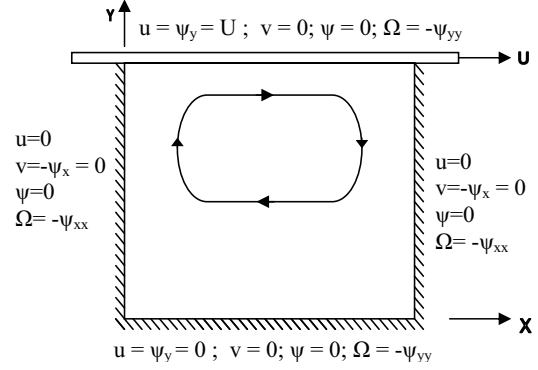

 Figure 14: Field variable contours for $Pe = 10^6$


Figure 15: Boundary conditions for cavity flow

Employing the Taylor series for ψ_i :

$$\psi_i = \psi_w - l \left(\frac{\partial \psi}{\partial n} \right)_w + \frac{1}{2} l^2 \left(\frac{\partial^2 \psi}{\partial n^2} \right)_w - \frac{1}{6} l^3 \left(\frac{\partial^3 \psi}{\partial n^3} \right)_w + O(l^4) \quad (35)$$

Ignoring the 4th order terms and higher and substituting Neumann B.C. for ψ on the wall as ($u=v=0$) one obtains

$$\frac{\partial \psi}{\partial \mathbf{n}} = \frac{\partial \psi}{\partial x} n_x + \frac{\partial \psi}{\partial y} n_y = -u n_x + v n_y = 0 \quad (36)$$

Considering Eqs. 34 and 36, Eq. 35 is written as below

$$\left(\frac{\partial^3 \psi}{\partial n^3} \right)_w = \frac{6}{l^3} \left(\psi_w - \psi_i - \frac{1}{2} l^2 \Omega \right) + O(l) \quad (37)$$

Applying the 1st order Euler scheme for the left hand side

$$\begin{aligned} \left(\frac{\partial^3 \psi}{\partial n^3} \right)_w &= \frac{(\partial^2 \psi / \partial n^3)_l - (\partial^2 \psi / \partial n^2)_w}{l} \\ &= \frac{\Omega_l - \Omega_w}{l} \end{aligned} \quad (38)$$

leads to the following equation:

$$\Omega_w = \frac{3}{l^2} (\psi_w - \psi_i) - \frac{1}{2} \Omega_l + O(l^2) \quad (39)$$

The above Equation is utilized for non moving boundaries (left, right and bottom) and obviously

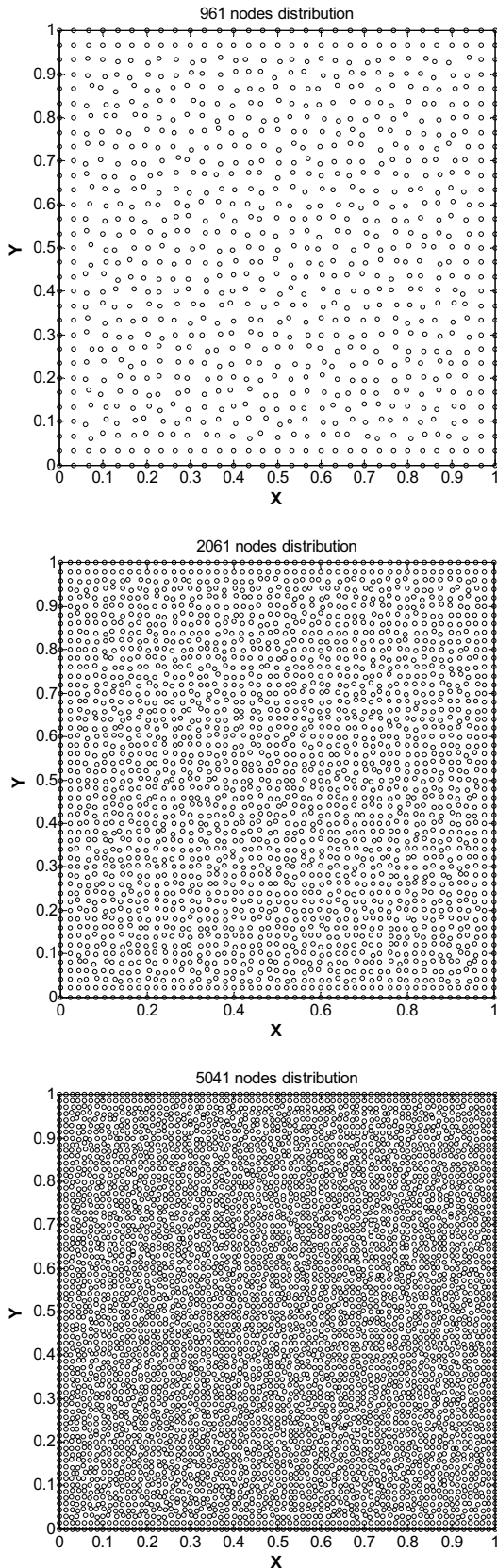


Figure 16: Domain with three nodal densities

it is of Dirichlet type. Apparently, the approximation is of 2^{nd} order accuracy. For the top boundary, where $U = \partial\psi/\partial n$, Eq. 35 is simplified to:

$$\left(\frac{\partial^3\psi}{\partial n^3}\right)_w = \frac{6}{l^3} \left(\psi_w - \psi_i - \frac{1}{2}l^2\Omega - lU\right) + O(l) \quad (40)$$

And similar to Eq. 39, the vorticity boundary condition for the moving boundary is finally obtained as:

$$\Omega_w = \frac{3}{l^2}(\psi_w - \psi_i) - \frac{1}{2}\Omega_i - \frac{3}{l}U + O(l^2) \quad (41)$$

Hence, the utilized boundary conditions are summarized as

$$\Omega_w = \frac{3}{l^2}(\psi_w - \psi_i) - \frac{1}{2}\Omega_i + O(l^2) \quad (\text{Left, Right, Bottom})$$

$$\Omega_w = \frac{3}{l^2}(\psi_w - \psi_i) - \frac{1}{2}\Omega_i - \frac{3}{l}U + O(l^2) \quad (\text{Top})$$

Obviously, all boundary conditions are of Dirichlet type.

The boundary conditions associated with the well-known cavity problem is depicted in Fig. 15.

The top wall is moving horizontally with a constant velocity which drives a large recirculation region inside the cavity. With increasing moving wall velocity and hence the Reynolds number value, additional smaller recirculation zones appear in the corners of the cavity. In order to certify the described modified MLPG with radial basis functions, this case is studied for different values of Reynolds number and compared with verified data in this field. Domains with three nodal distributions are illustrated in Fig. 16.

8 Results

Problem with Reynolds number of up to $Re=1000$ were performed on the 961 nodal density domain. This nodal density was chosen to obtain a smooth solution in which circulations are evident, although convergent solutions were obtained in a 441-node domain. For Reynolds number of

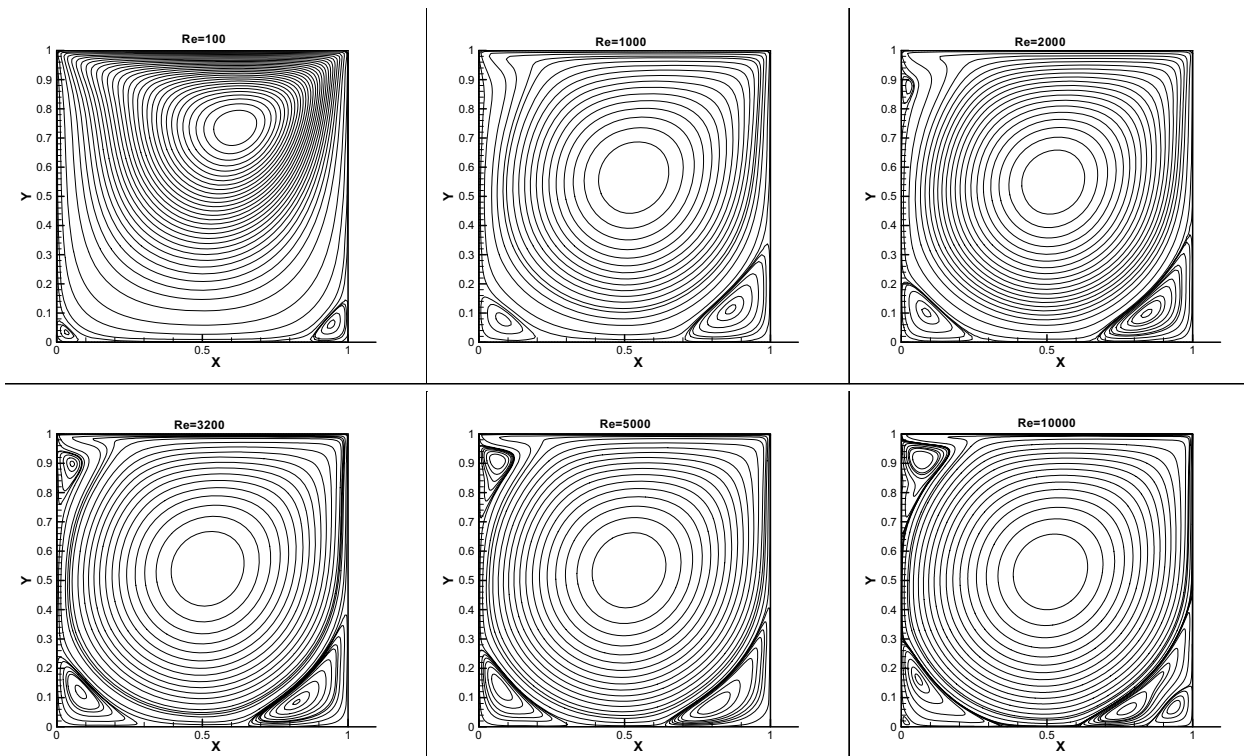


Figure 17: Stream function isolines

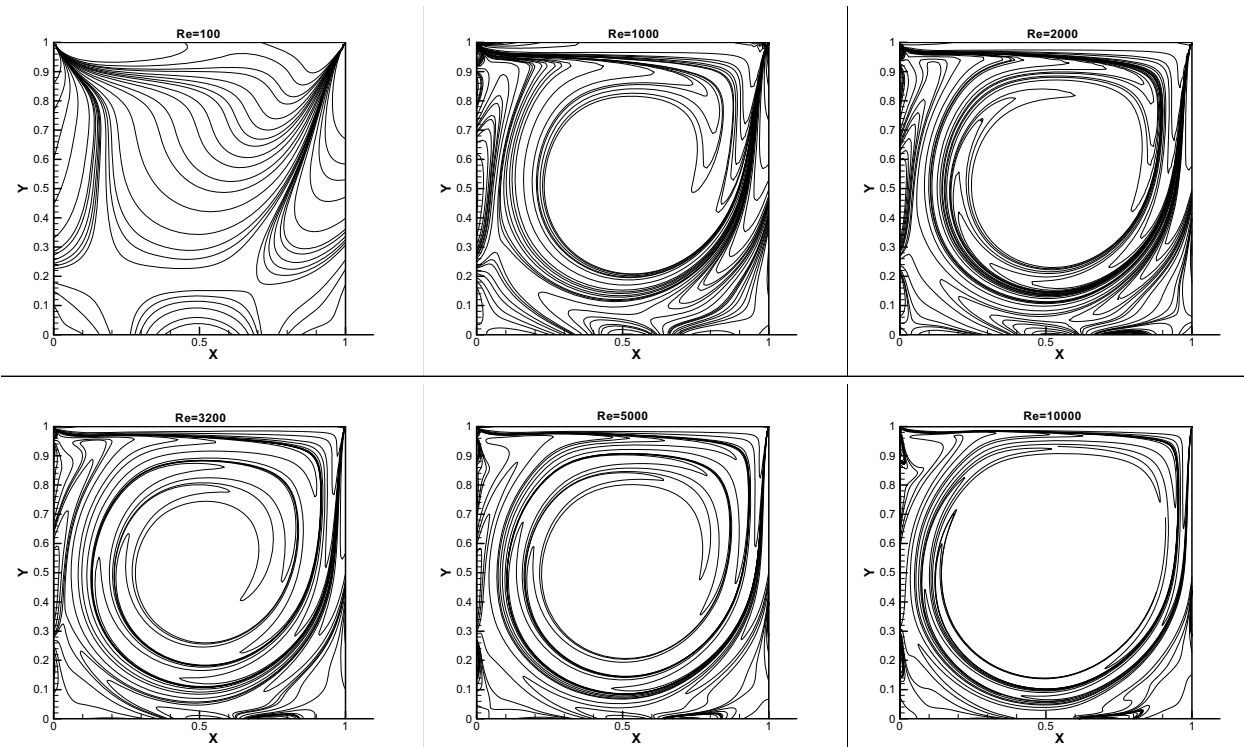


Figure 18: Vorticity contours

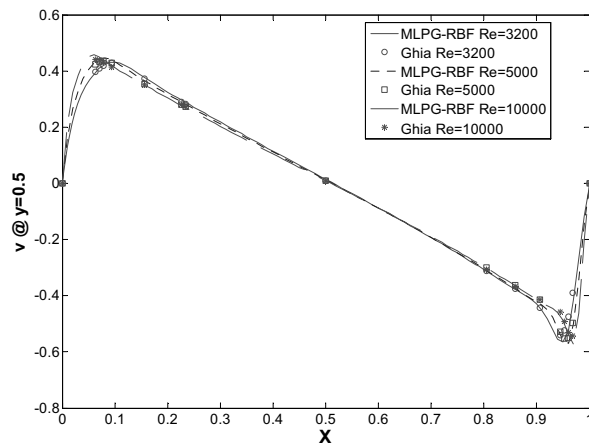
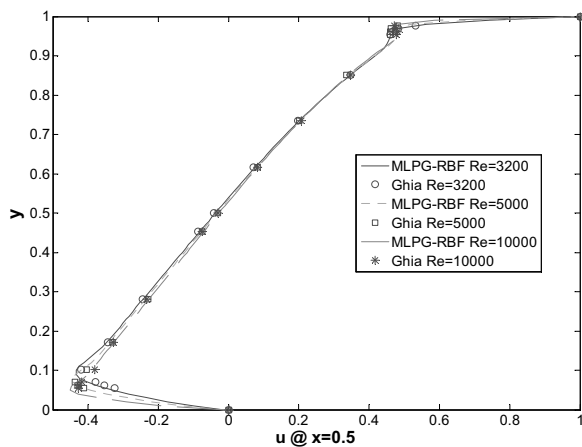
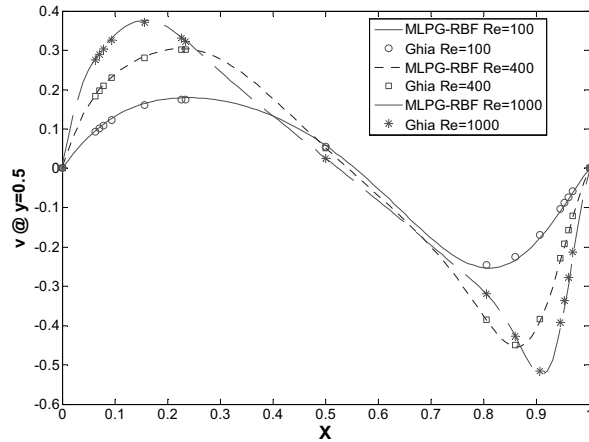
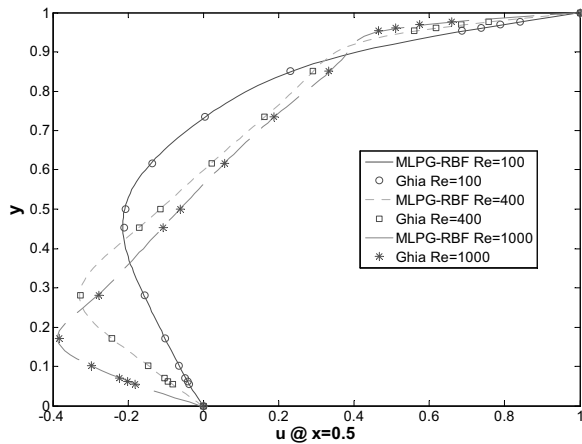


Figure 19: Comparison of horizontal velocity (u) on $x=0.5$

Figure 20: Comparison of vertical velocity (v) on $y=0.5$

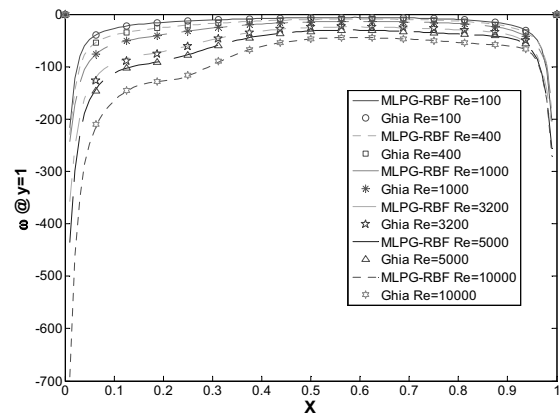


Figure 21: Comparison of vorticity (ω) on the moving wall

the nature of eddies, domain with 5041 nodes where employed for $Re=5000, 10000$.

The vorticity contours and streamlines for different values of Reynolds number are presented in Figs. 17 and 18, respectively.

As shown, the circulating nature of flow is intensified and more secondary eddies appear at corners as Reynolds number increases. To verify the solutions, results from current MLPG-RBF are compared to that of Ghia, U.; Ghia, K. N. and Shin (1982). In that article they presented velocity components on centerlines and vorticity on the top wall. Here, Multiquadric radial basis function with support size of $\alpha_s = 4.2$ is employed to obtain the values on centerlines. The comparisons are shown in Figs. 19, 20 and 21.

$Re=2000, 3200, 5000$ we obtained a convergent solution in a 2601-node domain. To demonstrate

Pressure field can be obtained by the pressure poisson Eq. 18. Neumann boundary condition is

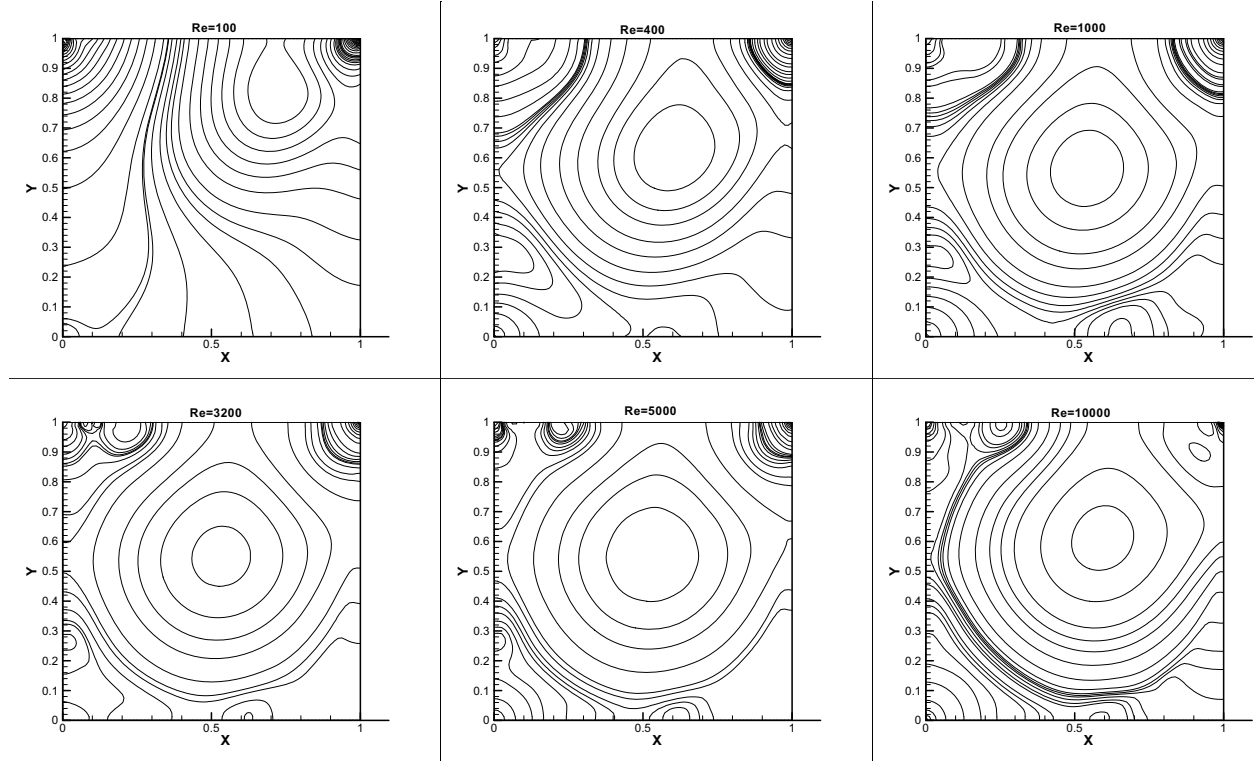


Figure 22: Pressure contours for different Reynolds numbers

imposed all over the global boundary except at the bottom left corner where pressure is considered to be zero. Pressure contours obtained by MLPG in 2061-nodal domain are illustrated in Fig. 22.

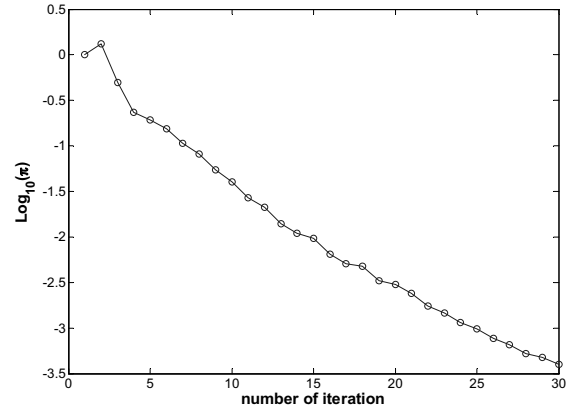
Obviously, the obtained pressure fields are smooth since MQ radial basis function is employed as interpolation technique. Consequently body force term (second order derivatives) is evaluated more accurately and stable solution is obtained while inaccurate values are obtained in most methods.

In order to study the rate of convergence, criterion (42) is adopted and calculated in each time step.

$$\Pi = \frac{\sum_{j=1}^{N_e} ({}^{k+1}\{\omega_j\} - {}^k\{\omega_j\})^2}{\sum_{j=1}^{N_e} ({}^{k+1}\{\omega_j\})^2} \quad (42)$$

The convergence for $Re=5000$ is plotted in Fig. 23.

Obviously, the solution has a monotonic and high convergence that it reaches to $\Pi = 10^{-6}$ in only

Figure 23: The convergence for $Re=5000$

109 iterations while other methods need a large number of iterations to reach steady state conditions. For instance, as noted in Zienkiewicz and Taylor (2000), about 48000 iterations are needed in FEM for $Re=5000$.

9 Conclusion

In this paper, meshless MLPG method with radial basis function is extended to fluid flow problems via a new stabilization technique. The technique was validated for a problem and compared to other existing techniques. It showed better performance and accuracy. The shape parameters of Multiquadric RBF were tuned and optimal values of MLPG parameters were determined. The benchmark problem of lid driven cavity flow was considered and solved with the mentioned upwinding scheme. Comparison of results for velocity and vorticity with that of other verified results showed excellent coincidence. The pressure fields were computed which showed satisfactory and free of oscillatory solutions. Also in the MLPG-RBF much less iterations were needed and solution converges more rapidly comparing to other methods.

References

- Arefmanesh, A.; Najafi, M.; Abdi, H.** (2008): Meshless local Petrov-Galerkin method with unity test function for non-isothermal fluid flow. *CMES: Computer Modeling in Engineering & Sciences*, vol.25, no.1, pp. 9-22.
- Atluri, S.N.; Liu, H.T.; Han, Z.D.** (2006): Meshless local Petrov-Galerkin (MLPG) mixed collocation method for elasticity problems. *CMES: Computer Modeling in Engineering & Sciences*, vol. 14, no. 3, pp. 141-152.
- Atluri, S.N.; Shen, S.** (2002): The meshless local Petrov-Galerkin (MLPG) method: a simple & less-costly alternative to the finite element and boundary element methods. *CMES: Computer Modeling in Engineering & Sciences*, vol. 3, no. 1, pp. 11-52.
- Atluri, S.N.; Zhu, T.** (1998): A new meshless local Petrov-Galerkin (MLPG) approach in computational mechanics. *Comput. Mech.*, vol. 22, pp. 117-127.
- Atluri, S.N.; Zhu, T.** (2000): New concepts in meshless methods. *Int. J. Numer. Methods Eng.*, vol. 47, pp. 537-556.
- Atluri, S.N.; Shen, S.** (2002): The meshless local Petrov-Galerkin (MLPG) method. *Tech. Science Press*, USA.
- Babuska, I.; Melenk, J.M.** (1997): The partition of unity method. *Int. J. Numer. Methods Eng.*, vol. 40, pp. 727-758.
- Belytschko, T.; Lu, Y.Y.; Gu, L.** (1994): Element free Galerkin methods. *Int. J. Numer. Methods Eng.*, vol. 37, pp. 229-256.
- Chantasiriwan, S.** (2006): Performance of multiquadric collocation method in solving lid-driven cavity flow problem with Low Reynolds Number. *CMES: Computer Modeling in Engineering & Sciences*, vol. 15, no. 3, pp. 137-146.
- Daux, C.; Mose, N.; Dolbow, J.; Sukumar, N.; Belytschko, T.** (2000): Arbitrary branched and intersecting cracks with the extended finite element method. *Int. J. Numer. Methods Eng.*, vol. 48, pp. 1741-1760.
- De, S.; Bathe, K.J.** (2000): The method of finite spheres. *Comput. Mech.*, vol. 25, pp. 329-349.
- Erturk, E.; Corke, T. C.; Gokcol, C.** (2005): Numerical solutions of 2-D steady incompressible driven cavity flow at high Reynolds numbers. *Int. J. Numer. Methods fluids*, vol. 48, pp. 747-774.
- Ghia, U.; Ghia, K.N.; Shin, C.T.** (1982): High-resolution for incompressible flow using the Navier-Stokes equations and multigrid method. *J. Comput. Phys.*, vol. 48, pp. 387-411.
- Gingold, R.A.; Monaghan, J.J.** (1977): Smoothed particle hydrodynamics: theory and application to non-spherical stars. *Monthly notices of the royal astronomical society*, vol. 181, pp. 375-389.
- Haji Mohammadi, M.; Shamsai, A.** (2006): Meshless solution of 2D fluid flow problems by subdomain variational method using MLPG method with radial basis functions. *ASME, Proceedings of FEDSM2006*.
- Han, Z.D.; Liu, H.T.; Rajendran, A.M.; Atluri, S.N.** (2006): The applications of Meshless Local Petrov-Galerkin (MLPG) approaches in high-speed impact, Penetration and Perforation Problems. *CMES: Computer Modeling in Engineering & Sciences*, vol.14, no.2, pp.119-128.
- Hoo, Y.K.** (2004): Study of radial basis functions

(RBFs) in mesh-free methods, *FYP Report*, Department of mechanical engineering national university of Singapore.

Jarak, T.; Sorić, J.; Hoster, J. (2007): Analysis of shell deformation responses by the meshless local Petrov-Galerkin (MLPG) approach. *CMES: Computer Modeling in Engineering & Sciences*, vol. 18, no. 3, pp. 235-246.

Kosec, G.; Sarler, B. (2008): Local RBF collocation method for Darcy flow. *CMES: Computer Modeling in Engineering & Sciences*, vol. 25, no. 3, pp.197-207.

Lin, H.; Atluri, S.N. (2000): Meshless Local Petrov-Galerkin (MLPG) method for convection-diffusion problems. *CMES: Computer Modeling in Engineering & Sciences*, vol. 1, no. 2, pp. 45-60.

Lin, H.; Atluri, S.N. (2001): The meshless local Petrov-Galerkin (MLPG) method for solving incompressible Navier-Stokes equations. *CMES: Computer Modeling in Engineering & Sciences*, vol. 2, no.2, pp. 117-142.

Liu, W.K.; Jun, S.; Zhang, Y.F. (1995): Reproducing kernel particle methods. *Int. J. Numer. Methods Eng.*, vol. 20, pp. 1081-1106.

Long, S.; Atluri, S.N. (2002): A meshless local Petrov-Galerkin method for solving the bending problem of a thin plate. *CMES: Computer Modeling in Engineering & Sciences*, vol.3, no.1, pp. 53-63.

Ma, Q.W. (2005): Meshless local Petrov-Galerkin method for two dimensional nonlinear water wave problems. *J. Comput. Physics*, vol. 205, pp. 611-625.

Ma, Q.W. (2008): A new meshless interpolation scheme for MLPG_R method. *CMES: Computer Modeling in Engineering & Sciences*, vol. 23, no. 2, pp. 75-89.

Moulinec, C.; Issa, R.; Marongiu, J.C.; Violeau, D. (2008): Parallel 3-D SPH simulations. *CMES: Computer Modeling in Engineering & Sciences*, vol.25, no.3, pp.133-147.

Nayroles, B.; Touzot, G.; Villon, P. (1992): Generalizing the finite element method: Diffuse approximation and diffuse elements. *Computational*

Mech., vol. 10, pp. 307-318.

Onate, E.; Idelsohn, S.; Zienkiewicz, O.C.; Taylor, R.L. (1996): A finite point method in computational mechanics applications to convective transport and fluid flow. *Int. J. Numer. Methods Eng.*, vol. 39, pp. 3839-3866.

Sarler, B. (2005): A radial basis function collocation approach in computational fluid dynamics. *CMES: Computer Modeling in Engineering & Sciences*, vol. 7, no. 2, pp. 185-193.

Shu, C.; Ding, H.; Yeo, K. (2005): Computation of incompressible Navier-Stokes equations by local RBF-based differential quadrature method. *CMES: Computer Modeling in Engineering & Sciences*, vol. 7, no. 3, pp. 195-206.

Sladek, J.; Sladek, V.; Atluri, S.N. (2004): Meshless local Petrov-Galerkin method for heat conduction problem in an anisotropic medium. *CMES: Computer Modeling in Engineering & Sciences*, vol. 6, no. 3, pp. 309-318.

Vavourakis, V.; Polyzos, D. (2007): A MLPG4 (LBIE) formulation in elastostatics. *CMC: Computers, Materials & Continua*, vol. 5, no. 3, pp. 185-196.

Vavourakis, V.; Sellountos, E.J.; Polyzos, D. (2006): A comparison study on different MLPG (LBIE) formulations. *CMES: Computer Modeling in Engineering & Sciences*, vol.13, no.3, pp.171-183.

Wendland, H. (1995): Piecewise polynomial positive definite and compactly supported radial basis functions of minimal degree. *Adv. Comput. Math.*, vol. 4, pp. 389-396.

Wu, X.; Shen, S.; Tao W. (2007): Meshless Local Petrov-Galerkin collocation method for two-dimensional heat conduction problems. *CMES: Computer Modeling in Engineering & Sciences*, vol. 22, no. 1, pp. 65-76.

Wu, Y.L.; Liu, G.R.; Gu, Y.T. (2005): Application of meshless local Petrov-Galerkin (MLPG) approach to simulation of incompressible flow. *Numerical Heat Transfer*, vol. 48, pp. 459-475.

Wu, Z. (1995): Compactly supported positive definite radial functions. *Adv. Comput. Math.*, vol. 4, pp. 283-292.

Xiao, J.R. (2004): Local heaviside weighted MLPG meshless method for two-dimensional solids using compactly supported radial basis functions. *Comput. Methods Appl. Mech. Eng.*, vol. 193, pp. 117-138.

Zhang, X.; Song, K.Z.; Lu, M.W.; Liu, X.H. (2000): Meshless methods based on collocation with radial basis functions. *Comput Mech.*, vol. 26, pp. 333-343.

Zhu, T.; Zhang, J.D.; Atluri, S.N. (1998): Local boundary integral equation (LBIE) method in computational mechanics and a meshless discretization approach. *Comput. Mech.*, vol. 21, pp. 223-235.

Zienkiewicz, O.C.; Taylor, R.L. (2000): The finite element method. *volume 3: Fluid Dynamics*, Butterworth-Heinemann, 5th edition.